Article

Displacement detection decoupling in counter-propagating dual-beams optical tweezers with large-sized particle

Xunmin Zhu [1], Nan Li [1,*], Jianyu Yang [1], Xingfan Chen [1,2] and Huizhu Hu [1,2,*]

[1] State Key Laboratory of Modern Optical Instrumentation, College of Optical Science and Engineering, Zhejiang University, Hangzhou 310027, China; 11630014@zju.edu.cn (X.-M.Z); 3160101439@zju.edu.cn (J.-Y.Y); mycotty@zju.edu.cn (X.-F.C)

[2] Quantum Sensing Center, Zhejiang Lab, Hangzhou, 310000, China

* Correspondence: nanli@zju.edu.cn (N.L.); huhuizhu2000@zju.edu.cn (H.-Z. H)

Abstract: Optical tweezers, as a kind of ultra-sensitive acceleration sensing platform, show a minimum measurable value inversely proportional to the square of the diameter of the levitated spherical particle. However, the coupling of the displacement measurement between axes becomes notable, along with the increasing of the diameter. This paper analyzes the source of coupling in a forward scattering far-field detection regime and proposes a novel method of suppression. We theoretically and experimentally demonstrated that when three variable irises added into detection optics, without changing other parts of optical structures, the decoupling of triaxial displacement signals mixed with each other show significant improvement. The detection coupling ratio reduction of 49.1 dB and 22.9dB has been realized in radial and axial direction respectively, which is principally in accord with simulations. This low cost and robust approach makes it possible to accurately measure three-dimensional mechanical quantities simultaneously and even go further such as active cooling the particle to quantum ground state.

Keywords: optical tweezers; optical trap; acceleration; decoupling

1. Introduction

Optical tweezers (OT), as an intriguing tool in various areas such as cell biology, weak mechanics sensing and quantum physics, enjoys increasingly attractive prospects [1-3]. A particle levitated in OT is isolated from the thermal noise of clamping, which is a fundamental, unavoidable source of dissipation in a traditional mechanical oscillator [4, 5]. Moreover, the optical interference method can be easily used in OT to measure displacement with excellent spatial and temporal resolution. Therefore, OT in high-vacuum can measure ultra-weak acceleration up to the nano-g scale, as the state of art level in a mechanical sensing application [4]. There are many proposals and experiments in exploring fields including non-Newtonian gravitation at sub-millimeter length scales, as well as the precise measurement of static characteristics and temporal variations of earth gravity [6, 7].

The minimum measurable acceleration in OT is inversely proportional to the square of the diameter of the spherical levitated particle. At present, there are two OT schemes for levitating large-sized particles: a single vertically upward beam or horizontal counter-propagating dual-beams. In the former scheme, axial radiation pressure is balanced with gravity on the particle, while pressures of the two beams cancel out in the latter scheme. The maximum diameter of particle currently levitated in the two solutions is 14μm [8] and 10μm [9], respectively. However, the latter can levitate larger particles theoretically, due to radial radiation pressure being stronger than axial one. Moreover, it has an applicability of working in a microgravity environment.

Owing to its axial symmetry, the particle centroid is naturally on the optical axis in OT with a single beam and a spherical particle, but this is not true in misaligned OT with multi-beams.

Misalignment leads to the motion information of one axis to be coupled to another in displacement detection. Coupling becomes notable as particle size increases and comes near to beam waist [10]. To a certain extent, it limits acceleration detection performance. Unfortunately, it is challenging to ensure the coaxiality of counter-propagating beams. Aiming focuses of two beams at the same pinhole is commonly used for alignment in OT. However, a radial alignment error (RAE) of only about 1 μm can be reached due to restriction by the coaxiality of the tubular pinhole and the two beams. This error is defined as the distance between the particle centroid and the optical axis when forces on it are balanced. Increasing beam waist can weaken coupling, but it also drastically reduces detection sensitivity. Furthermore, detection, already restricted by other noises such as Johnson noise, deteriorates seriously. Response bandwidth also decreases and the chance of applying OT in realms of high-speed particle motion is missed.

Although a spherical particle of 3μm in diameter [11, 12] or 10μm [9] has been levitated in experiments in OT of dual-beams, the maximum diameter according to theoretical research on particle translation detection regime is only 1μm [10]. We chose to suspend a ball of 10μm in diameter both in the simulation and the experiment in OT of dual-beams. Moreover, its coupling was analyzed with forward scattering far-field images acquired by the Fresnel diffraction method. There is a novel method proposed to suppress coupling, adding a variable iris in front of the photo-detector on each axis. Experiments show a reduction of 49.1 dB in detection coupling ratio radially and that of 22.9 dB axially, which basically corresponds with simulations. These make it possible to accurately measure three-dimensional mechanical quantities with OT simultaneously and do further operations beyond it such as active cooling the particle to quantum ground state in low gas pressure in basic physics research. Moreover, the original optical structures of levitation and detection do not need to be changed, because these three variable irises are set just behind all optical components in OT. A laser beam profiler is also employed for the temporary recording of far-field images. Importantly, the above methods have advantages of low cost and good structural compatibility.

2. Theory

2.1. Displacement detection and coupling

Most mechanical quantities to be measured in OT are directly related to the levitated particle centroid displacement detection. The displacement detection methods mainly fall into two camps: recording far-field interference images directly [13, 14] with sensors such as CCD or measuring the intensity of each part of the far field interference image with sensors such as four-quadrant photo-detectors (QPD) and a balanced photo-detector (BD) [10, 11, 15, 16]. Although the former can obtain more information from the image, its detection sensitivity is impaired by a time-consuming image transmission and process. Thus, the latter one should only be used when pursuing a detection of ultra-low mechanical quantities.

The typical QPD scheme of particle centroid displacement detection in OT is shown in Figure 1. If the optical radiation force for levitating particles is provided by beam No. 1 only, it is then called single beam OT. In contrast, sometimes there is a counter-propagating beam No.2. This is reflected by BS and focused by a condenser, thus forming counter-propagating dual-beam OT.

Preprints (www.preprints.org) | NOT PEER-REVIEWED | Posted: 21 July 2020 doi:10.20944/preprints202007.0496.v1

Peer-reviewed version available at Sensors 2020, 20, 4916; doi:10.3390/s20174916

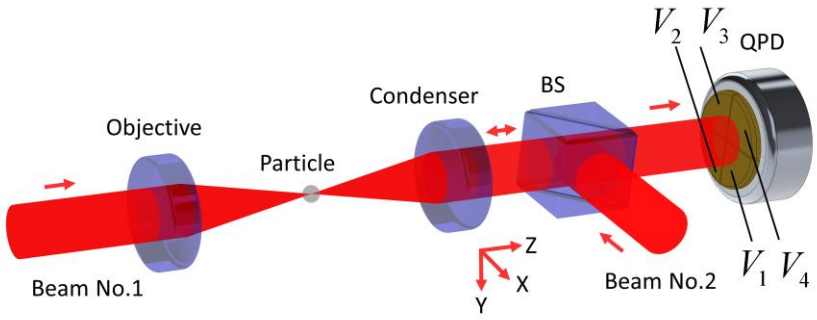

Figure 1. Typical QPD scheme of particle centroid displacement detection in OT. Beam No. 1 is incident on the particle after being focused by the objective, whose focus approximately coincides with the condenser, thus incident light and forward scattered light are both collected by the condenser. Once they have passed through the beam splitter (BS), a far-field interference image is formed on the photosensitive surface (yellow) of the QPD.

As shown in Figure 1, one radial direction of beam is defined as the x-axis, and the beam propagates along the positive z direction. This set of coordinates is always used below. Assuming that the voltages obtained by converting light intensity on the four photosensitive surfaces are V_k, values for $k = 1\ to\ 4$, respectively. Supposing $V_T = V_1 + V_2 + V_3 + V_4$, the final detection response of each axis will be [12]:

$$\begin{cases} V_x = \dfrac{V_1 - V_2 - V_3 + V_4}{V_T} < V_T > \\ V_y = \dfrac{V_1 + V_2 - V_3 - V_4}{V_T} < V_T >, \\ V_z = V_T - < V_T > \end{cases} \tag{1}$$

where symbol <> means time-domain average. The response of BD is the same as of QPD, while smaller photosensitive surfaces are used for detection at higher bandwidths and of lower electricity noises. For convenience, only the QPD method will be discussed below.

Assuming that V_{ij} is i-axis detection response resulting from j-axis motion, $i = $ x, y, z and $j = $ x, y, z are always applicable hereinafter if not mentioned. The above total response of i-axis detector can be expressed as:

$$V_i = \sum_{j=x,y,z} V_{ij}. \tag{2}$$

The levitated particle in OT is always collided by the surrounding gas molecules, thereby generating irregular thermal motion. It's a kind of main noise source of displacement detection under relatively high gas pressure. The thermal motions of the particles on three-axis are all random and uncorrelated to each other. The motion information of other axes will become noise in the displacement detection signal of one specific axis. It is not easy to separate the three-axis motion information from the voltage output on one displacement detector. That's difficult especially for large-sized particle because its main motion component occupies the zero frequency area on all three axes. The definition of i-axis detection coupling ratio resulting from j-axis motion will then be:

$$R_{ij} = \frac{\langle V_{ij}^2 \rangle}{\langle V_{ii}^2 \rangle},\ i \neq j. \tag{3}$$

The logarithmic form $R_{ij}(\mathrm{dB}) = 10\log_{10} R_{ij}$ is often used there. There are six items for tri-axial displacement detection coupling, but only R_{xy}, R_{xz} and R_{zx} need to be considered owing

to axial symmetry. In general, the motion range of the particle centroid does not exceed the micrometer scale, and is much smaller than the beam waist of several micrometers. Therefore, the detection response is nearly linear with displacement. The *j*-axis motion detection sensitiv ity of *i*-axis detector is defined as:

$$\beta_{ij} = V_{ij} / x_j , \tag{4}$$

where x_j is the particle displacement of *j*-axis.

2. Materials and Methods

2.1. Setup in simulations and Experiments

We use the same structure explained in Figure 1 with dual-beams in simulations and experiments. The silica microsphere diameter is 10μm. Other parameters are as follows: the numerical aperture (NA) of objective and condenser are both 0.15; laser wavelength in vacuum λ is 1.064 μm; the ambient medium is air, thus its refractive index $n_{\mathrm{med}} = 1$. Consequently, the diameter of incident beam waist is about 4.5μm. The focal length of condenser f_1 and objective f_2 are both 18.4mm. The QPD is placed 0.2m behind the condenser. In the OT structure we used, the intensity of each beam is 800mW. The particle is nearly on the optical axis and is 10μm away from the focus, along the beam propagation direction.

2.2. Forward scattered far field computation

2.2.1. Computation principle

Increasing detection information is a feasible way to coupling suppression. The QPD method can only obtain the total intensities of four parts of the far-field interference image, while image recording methods are defective in accuracy by getting intensities of many points. Herein we try to find out the characteristics of a far-field interference image, which are more closely related to the positional change of a particle by a combination of simulation of and experiment on the QPD detection regime.

Triaxial QPD detection responses of OT with single Gaussian beam structure have been calculated by means of Rayleigh scattering [15, 16], Mie scattering [17] and the extended boundary condition method [10]. Only the last method can analyze large-sized particles up to several micrometers with acceptable time-space complexity of computation of about less than one day. It obtains the forward scattering near-field represented by spherical harmonics function [18]. Field values within a certain solid angle are then accumulated to get responses on the QPD. Coupling has been revealed in OT, where the diameter of laser beam and spherical particle was 0.43μm and 1μm, respectively [13]. However, it expresses far-field with endless distance approximation. Thus, an interference image at a limited distance cannot be acquired this way. We yield the interference image through twice Fresnel diffraction [19], as shown in Figure 2. The first diffraction is calculated with the single fast Fourier transform (SFFT) method, and the second one with the double fast Fourier transform (DFFT) method.

Preprints (www.preprints.org) | NOT PEER-REVIEWED | Posted: 21 July 2020 doi:10.20944/preprints202007.0496.v1

Peer-reviewed version available at Sensors 2020, 20, 4916; doi:10.3390/s20174916

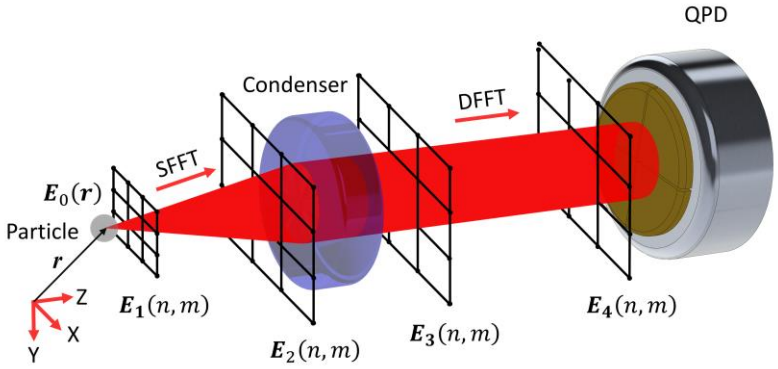

Figure 2. A schematic of obtaining the far-field interference image by twice Fresnel diffraction. First, near-field $E_0(\mathrm{r})$ is changed into sample values $E_1(\mathrm{n},\mathrm{m})$ in a Cartesian coordinate system. Secondly, field $E_2(\mathrm{n},\mathrm{m})$ on the front surface of condenser is calculated by the SFFT method. It is Then multiplied by the lens phase function and turns into $E_3(\mathrm{n},\mathrm{m})$. Finally, the interference image $E_4(\mathrm{n},\mathrm{m})$ is obtained by the DFFT method.

2.2.2. Computation complexity

For the OT structure we used, the derivation below shows that 253 instances of computation are needed if DFFT is chosen as the first Fresnel diffraction method compared with SFFT. Furthermore, nine instances of computation are required for SFFT compared with DFFT in the second diffraction. The lateral size of the main energy region (MER) near the particle is L_1, and is L_2 for far-field on the front surface of condenser. $L_2 \approx 2f_1\tan(\mathrm{asin}(\mathrm{NA}/n_{\mathrm{med}}))$. The number of sampling points both at the near and far field is N_s. The grid size of diffraction surface is L_3 while that of the observation surface is L_4. $L_4 = N_s\lambda L_5/L_3$ in the SFFT method where L_5 is diffraction distance and $L_5 = f_1$. $L_4 = L_3$ in the DFFT method. Therefore, two sets of conditions need to be met. First, the sampling space needs to cover MSR. Secondly, the number of sampling points in MSR is not less than N_{min}. Those are:

$$\begin{cases} L_3 \geq L_1 \\ L_4 \geq L_2 \\ N_s L_1 / L_3 \geq N_{\min} \\ N_s L_2 / L_4 \geq N_{\min} \end{cases}. \tag{5}$$

Values for N_s are at least 1800 and 100 in the first and second diffraction, respectively, when $N_{\min}$ is equal to 100.

2.2.3. Computation errors

The SFFT and DFFT methods are both based on scalar diffraction. Paraxial approximations should therefore be taken into account [20]. The intensity distribution of the image rather than the phase is concerned there, that is:

$$L_5 \gg L_6 = \sqrt{2(L_2/2)^2}/2. \tag{6}$$

L_5 is 18.4mm and L_6 equals to 0.2mm in OT structure we used. The grid size of diffraction surface also needs to be much larger than wavelength, hence:

$$L_3 \gg \lambda. \tag{7}$$

L_5 is 350μm and λ equals to 1.064μm in OT structure we used.

Only the forward scattered field is considered above, while the backward field of the second beam is ignored in OT with counter-propagating beams. Simulation shows that backward field

intensity is two orders of magnitude lower than that of the forward one because of the low refractive index and Mie scattering state.

3. Simulations

3.1. Simulation of computing forward scattered far field

For the OT structure we used, images in Figure 3(a) show the simulation results for the far-field interference image when the particle moves the distance Δ_x along the x-axis. The factor Δ_x is just the RAE mentioned above. Images in Figure 3(b) are simulation results for the scenario when particle moves the distance Δ_z along the z-axis. The particle is on the optical axis, and is 10μm away from the focus of Beam No.1 when $\Delta_x = 0$ and $\Delta_z = 0$. More specifically, the particle is closer to the condenser compared with the focus of Beam No.1. Curves in Figure 3(c) are the normalized laser intensity distributions of the interference image in horizontal cross-section in Figure 3(a), whereas curves in Figure 3(d) are those of Figure 3(b) by the same token.

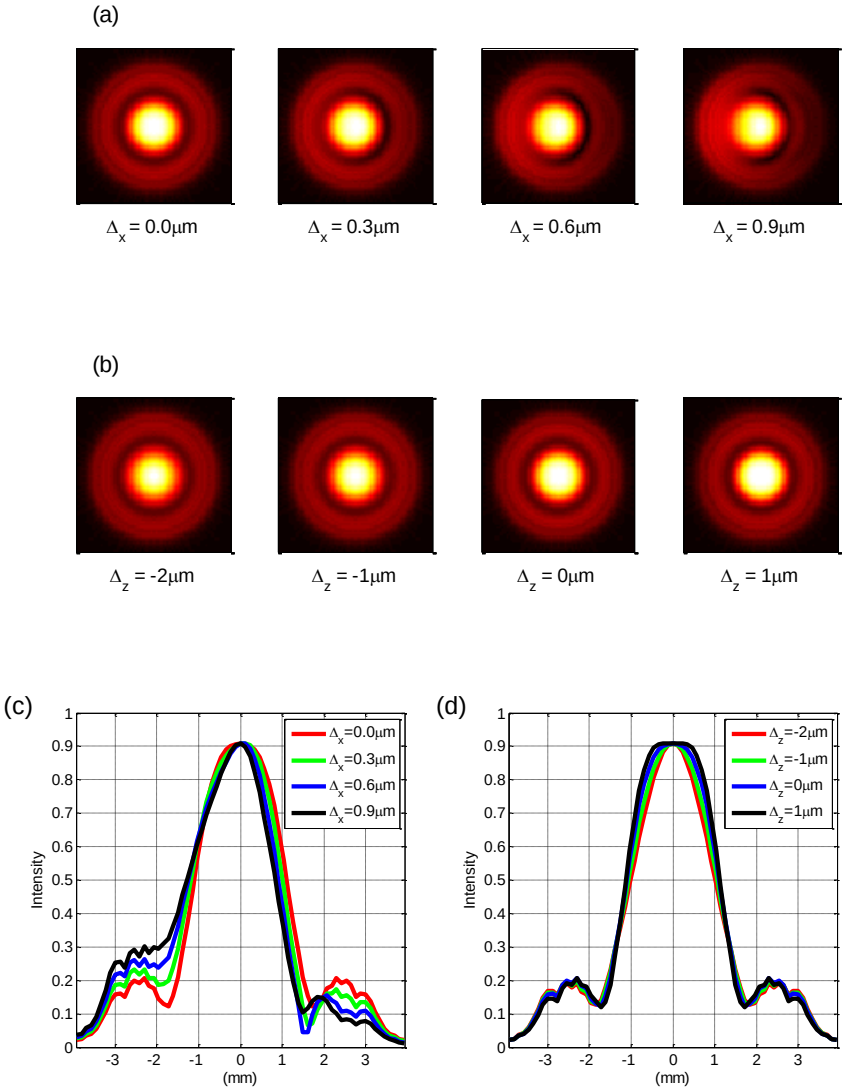

Figure 3. (a) Far-field interference images in simulation under different radial displacements of particle. (b) Far-field interference images under axial displacements. (c) Horizontal cross-section of (a). (d) Horizontal cross-section of (b).

It can be seen from Figure 3(a) and 3(c) that the interference image is similar to an Airy disk when the particle is exactly on the optical axis. These images all have a bright spot and ring with an

outer diameter of about 8mm. Conversely, only the spot is present if particle size is much smaller than beam waist, which can be explained qualitatively by the diffraction principle. The spot is shifted to left side when the particle moves right, but the ring stays in place. It is clear from Figure 3(c) that the ring intensity increases on the left and decreases on the right, while spot intensity is almost fixed. Based on Figure 3(d), the intensities of the spot and the ring both gradually decrease when the particle moves along the beam propagation direction. The former changes more obviously, while their central positions remain unchanged. Since images in Figure 3(a) reflect RAE directly, they can also instruct alignment, as well as monitor structural changes in OT.

3.2. Simulation of decoupling with the modified QPD method

A difference in laser intensity between the two halves of the interference image corresponds to a radial signal in QPD. Neither the spot nor the ring in the image is divided equally by QPD, when the particle is not on the optical axis as in Figure 3(a). Therefore, the radial detector responds to axial motion in that case. If an iris is set before QPD to filter out the ring and retain the spot in the image, the equally divided spot provides information of lateral motion only. The axial signal is derived by the total laser intensity variation of the image. When the particle is not on the optical axis, axial detection coupling occurs, since laser intensity changes on both sides of the ring cannot cancel each other out, as seen in Figure 3(c). The setting of an iris eliminates the ring and is expected to suppress this coupling.

Assuming that the two beams only have RAE in the x-axis direction in the OT structure we used, Figure 4(a) shows the relationship between RAE and R_{xz} when using the conventional QPD method and the modified QPD method in interference image simulation, with different iris diameters D_{iris}. Similarly, the relationship between RAE and R_{zx} is described in Figure 4(b). $R_{xy} = R_{yx}$ and their value is always no more than -80 dB even if the RAE deteriorates to 1 μm, thus no further analysis for them is provided below.

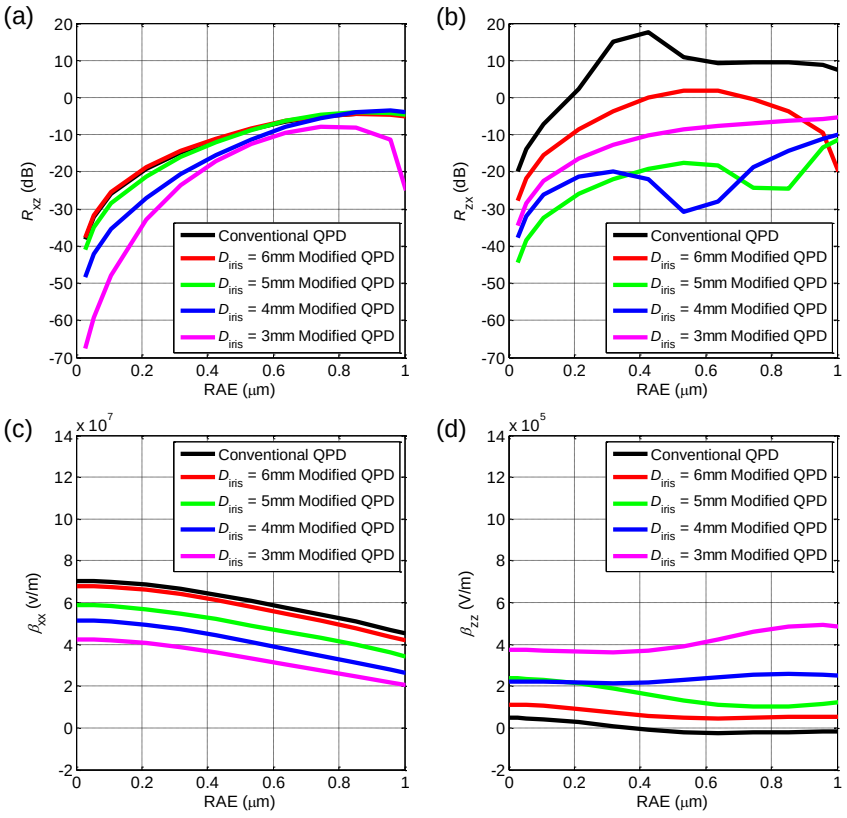

Figure 4. (a) The x-axis detection coupling ratio resulting from z-axis motion R_{xz} under different RAE in conventional QPD and modified QPD methods. (b) The relationship between the z-axis detection coupling ratio caused by x-axis motion R_{zx} and RAE in conventional QPD and modified

QPD methods. (c) The x-axis motion detection sensitivity of x-axis detector β_{xx} under different RAE values. (d) The relationship between the sensitivity of z-axis detector β_{zz} and RAE.

Detection coupling ratio R_{xz} and R_{zx} grow rapidly as RAE increases. When RAE reaches to 0.3μm in conventional QPD, these will increase to -16.7 dB and 13.5 dB, respectively,. When iris diameters in modified QPD are set to 3mm and 5mm, respectively, the values for coupling suppression are optimal radially and axially, reducing to -25.7 dB and -23.2 dB, respectively, when RAE equals to 0.3μm. That consists a diminution of coupling detection level up to 9.0 dB radially and 36.7 dB axially. As RAE increases, the amplitude of coupling repression also attenuates rapidly. This means that the modified QPD method can have a better coupling suppression effect, if the alignment is improved in advance. Figure 4(c) takes on the relationship between RAE and β_{xx}, while Figure 4(d) demonstrates that β_{zz}. β_{xx} decreases by about 6.6 dB, when using 3mm iris as an optimal diameter. Furthermore, β_{zz} increases by an order of magnitude only in modified QPD.

4. Experiments

4.1. Experiment of recording Forward scattered far field

The far-field interference image was recorded by a beam profiler as in Figure 5(a), with its vertical cross-section shown in Figure 5(b). In the latter figure, the cross-section (blue solid line) is compared with the simulation curve (red dotted line), when $\text{RAE} = \Delta_x = 0$. When considering the relative central position of the spot and the ring in Figure 5(a), RAE is no more than 0.3um. In the experiment, RAE was mainly concentrated in the horizontal direction and the spot was slightly down in the vertical direction. First, a pinhole of 5μm diameter was put into OT and we aimed the focuses of two beams at it. However, the thickness of the pinhole cannot be infinitely small, with the one we selected of about 50μm. It is difficult to guarantee a coaxiality of less than 1/25 radian and ensure at most 1μm RAE in free space by manual adjustment. The particle will be at the midpoint of the line connecting the focal points, assuming that the counter-propagating dual-beams are exactly the same. We used images in Figure 3(a) to instruct alignment, and then Figure 5(a) was acquired.

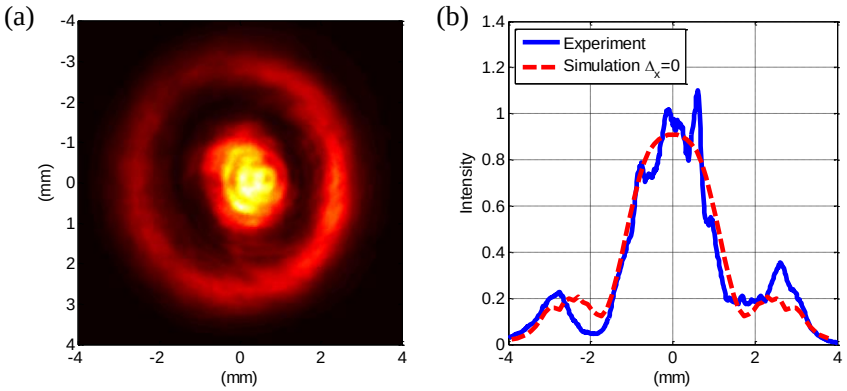

Figure 5. (a) Interference image before QPD in the experiment. (b) Vertical cross-section of (a) with the simulation curve.

4.2. Experiment of decoupling with the modified QPD method

A variable iris was placed in front of QPD on each axis in modified QPD method in experiments, as close to it as possible to reduce the diffraction effect. Simulations in Figure 4(a) and 4(b) indicate that the iris should eliminate the ring in the radial detection entirely, and keep half of that axially.

In theory, detection coupling ratio between axes $R_{ij}, i \neq j$ can be measured by exerting a known force on the levitated particle in OT. But it's not easy to implement in practice. The thermal motion of the particle in OT will drown out the known force signals that we applied under relatively high gas pressure. On the other hand, increasing the known force exerted may cause the particle to deviate too far from the linear response region of the QPD detection, to accurately measure the coupling ratio.

Preprints (www.preprints.org) | NOT PEER-REVIEWED | Posted: 21 July 2020 doi:10.20944/preprints202007.0496.v1

Peer-reviewed version available at Sensors 2020, 20, 4916; doi:10.3390/s20174916

In contrast, the displacement power spectrum (PSD) of the particle is a more convenient tool for checking the coupling ratio, as it's unnecessary to add devices of applying known forces into the OT and choosing the magnitude of the force carefully. Displacement PSD on the j-axis in OT can be described as [20]:

$$S_{xx,j}(\omega) = 2 < x_j^2 > f_L(\omega), \tag{8}$$

where $f_L(\omega)$ is the normalized Lorentz function: $\Omega_j^2\Gamma_0 / \left[\left(\Omega_j^2 - \omega^2\right)^2 + \omega^2\Gamma_0^2\right]$, Γ_0 is gas damping. and Ω_j is intrinsic angular frequency, which is close to angular frequency at the resonance peak in PSD. Next, the output voltage PSD of the i-axis motion detector, according to Equation 2 and Equation 4, is determined as follows:

$$S_{vv,i}(\omega) = \sum_{j=\mathrm{x,y,z}} \beta_{ij} S_{xx,j}(\omega). \tag{9}$$

The voltage PSD of the single axis detector shows multiple peaks when coupling results from the difference in Ω_j and irrelevance of motion between the axes. In general, Ω_z is much less than Ω_x. Thus, $\beta_{\mathrm{xx}}^2 S_{xx,\mathrm{x}}(\Omega_\mathrm{x}) \gg \beta_{\mathrm{xz}}^2 S_{xx,\mathrm{z}}(\Omega_\mathrm{x})$. When coupling is serious enough that $\beta_{\mathrm{xz}}^2 S_{xx,\mathrm{z}}(\Omega_\mathrm{z}) \gg \beta_{\mathrm{xx}}^2 S_{xx,\mathrm{x}}(\Omega_\mathrm{z})$, R_{xz} will be:

$$\frac{S_{vv,\mathrm{x}}(\Omega_\mathrm{z})}{S_{vv,\mathrm{x}}(\Omega_\mathrm{x})} \approx \frac{\beta_{\mathrm{xz}}^2 S_{xx,\mathrm{z}}(\Omega_\mathrm{z})}{\beta_{\mathrm{xx}}^2 S_{xx,\mathrm{x}}(\Omega_\mathrm{x})} = R_{\mathrm{xz}}. \tag{10}$$

On the contrary, only the upper limit of the coupling ratio can be obtained under mild coupling. The limit is:

$$R_{\mathrm{xz,max}} \approx \frac{\beta_{\mathrm{xx}}^2 S_{xx,\mathrm{x}}(\Omega_\mathrm{z})}{\beta_{\mathrm{xz}}^2 S_{xx,\mathrm{x}}(\Omega_\mathrm{x})} = \frac{\beta_{\mathrm{xx}}^2}{\beta_{\mathrm{xz}}^2 Q_x^2}, \tag{11}$$

where $\mathrm{Q}_j = \Omega_j/\Gamma_0 \gg 3$, and $j = \mathrm{x,y,z}$. The ratio R_{zx} follows the same derivation process as above, except that the equal sign needs to be changed into the less-than sign in Equation 11.

As a result, the reduction of gas pressure can lower the upper limit of PSD method for checking the coupling ratio. The reduction of gas pressure also wakens the collision thermal movement and improves the signal to noise ratio of the above exerting known force method. But the reduction of gas pressure can't go on all the time because the levitated particle is more likely to escape from the OT in lower gas pressure. In order to ensure the particle stably exist in OT under low pressure, and the mechanical energy of it is continuously reduced, we need to apply appropriate feedback force on the particle according to the position and velocity information of it. This is the so-called cooling. Apparently, the cooling effect depends partly on the accuracy of the particle position measurement, which is closely related to detection coupling.

Figure 6(a) shows $S_{vv,\mathrm{x}}(\omega)$ in logarithmic form with conventional QPD or the modified CPD method with an optimal iris diameter. That is, $S_{vv,\mathrm{x}}(\omega)\ (\mathrm{dB}) = 10\log_{10}\left[S_{vv,\mathrm{x}}(\omega)\right]$. And Figure 6(b) tells that of $S_{vv,\mathrm{z}}(\omega)\ (dB)$. The coupling ratio $R_{ij}, i \neq j$ is then exactly the height difference between peaks at frequency Ω_z and Ω_x along the same line in Figure 6(a) and 6(b).

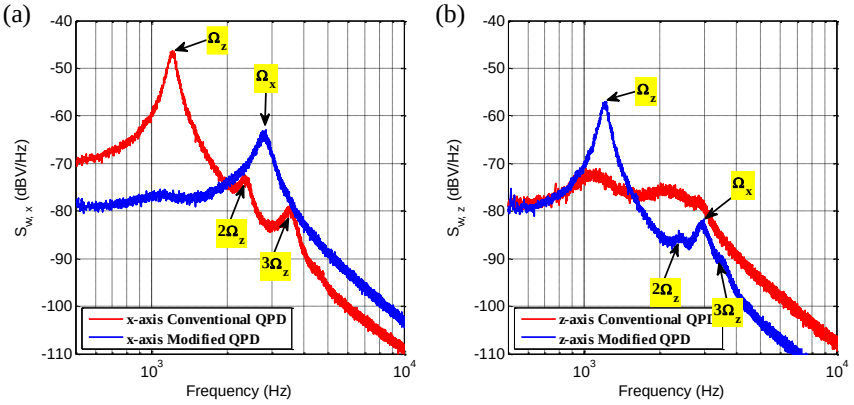

Figure 6. (a) Output voltage PSD of x-axis motion detector $S_{vv,x}(\omega)$ (dB) in conventional QPD and modified CPD method in experiment. b) That of $S_{vv,z}(\omega)$ (dB) in conventional QPD and modified CPD method in experiment.

When using modified QPD, R_{xz} was meliorated from 36.0 dB to -13.1 dB, and this method also reduced R_{zx} from -5.5 dB to -28.4 dB. That is, a reduction of detection coupling ratio occurs up to 49.1 dB radially and 22.9 dB axially. Signal strength increases by 14.3 dB axially around resonance peak, and decreases by 11.0 dB radially in the range of 500 Hz to 10 kHz. According to Fig. 6, there is no loss of bandwidth.

4. Discussion

Apart from misalignment, there are other factors that affect detection accuracy. When using conventional QPD methods, R_{xz} = 36.0 dB for the red line in Fig. 6 (a), that is much higher than that in the simulation, as in Fig 4 (a). This appears to be caused by asymmetric beam shape, increasing off-centering of the spot division in the interference image. The laser intensity on the right side of the ring in Fig. 5 (a) can confirm this, showing that modified QPD can suppress it and spatial filters may help to improve beam quality.

Voltages PSD of the red line in Fig 6 (a) and the blue line in (b) take on apparent second and third harmonics of the pretty large amplitude of z-axis motion. It indicates a nonlinear relation between V_{iz} and x_z. Nonlinearity is less than -25.1 dB for the second harmonic and -32.5 dB for the third one. Furthermore, it can be reduced by of other means of detection or by controlling the z-axis motion of the particle.

5. Conclusions

Overall, optical tweezers with counter-propagating beams and a large-sized particle is a technology with great potential, which is applicable in fields of research such as cell biology, weak mechanics sensing and quantum physics. However, its measurement accuracy faces challenges due to coupling of different axes. This paper proves that coupling is caused by misalignment from the perspective of the forward scattering far-field.

A new method of suppressing coupling is proposed herein, adding a variable iris in front of the QPD photo-detector on each axis. Experiments show a reduction of 49.1 dB in detection coupling ratio radially and that of 22.9 dB axially, which is basically in accord with simulations. These make it possible to accurately measure three-dimensional mechanical quantities with OT synchronously and even do further operations beyond it such as active cooling the particle to quantum ground state in ultra-low gas pressure in basic physics research. The measurements of bandwidth and signal strength do not suffer a great loss in these methods as opposed to those such as increasing beam diameter. A laser beam profiler and three variable irises are added into OT without changing the original optical structures of levitation and detection. Thus, they provide simple operation at a low cost and structural compatibility.

Supplementary Materials: The following are available online at www.mdpi.com/xxx/s1, Figure S1: title, Table S1: title, Video S1: title.

Author Contributions: Conceptualization, X.-M.Z and N. L.; methodology, X.-M.Z and X.-F.C; software, X.-M. Z and J.-Y.Y; validation, all authors; formal analysis, all authors; investigation, all authors; resources, H.-Z.H, X.-F.C and N.L; data curation, all authors; writing—original draft preparation, X.-M.Z; writing—review and editing, N.L.; visualization, all authors; supervision, H.-Z.H and N.L.; project administration, H.-Z.H and X.-F. C and N L.; funding acquisition, H.-Z. H, X.-F. C. and N. L. All authors have read and agreed to the published version of the manuscript.

Funding: This research was funded by Natural National Science Foundation of China (No. 11304282, 61601405), Joint Fund of Ministry of Education (No.6141A02011604), Major Scientific Research Project of Zhejiang Lab (No.2019MB0AD01) and National Program for Special Support of Top-Notch Young Professionals, Fundamental Research Funds for the Central Universities (2016XZZX004-01, 2018XZZX001-08).

Conflicts of Interest: The authors declare no conflict of interest.

References

1. Choudhary, D.; Mossa, A.; Jadhav, M.; Cecconi, C. Bio-Molecular Applications of Recent Developments in Optical Tweezers. *Biomolecules* **2019**, 29(1), 23.
2. Rider, A.D.; Moore, D.C.; Blakemore, C.P.; Louis, M.; Lu, M.; Gratta, G. Search for Screened Interactions Associated with Dark Energy Below the 100 μm Length Scale. *Phys. Rev. Lett.* **2016**, 117, 101101.
3. Ranji, G.; Cunningham, M.; Casey, K.; Geraci, A.A. Zeptonewton force sensing with nanospheres in an optical lattice. *Phys. Rev. A.* **2016**, 93, 053801.
4. Ashkin, A.; Dziedzic, J.M.; Bjorkholm, J.E.; Chu, S. Observation of a single-beam gradient force optical trap for dielectric particles. *Opt. Lett.* **1986**, 11, 288.
5. Neuman, K.C.; Block, S.M. Observation of a single-beam gradient force optical trap for dielectric particles. *Rev. Sci. Instrum.* **2004**, 75, 2787.
6. Erik, H.; Martin, F.; Rene´, R.; Lukas, N. Measuring gravity with optically levitated nanoparticles," *Advanced Photonics* **2018**, 12(9), 806-810.
7. Geraci, A.A.; Smullin, S.J.; Weld, D.M.; Chiaverini, J.; Kapitulnik, A. Improved constraints on non-Newtonian forces at 10 microns *Phys. Rev. D.* **2008**, 78, 022002.
8. Monteiro, F.; Ghosh, S.; Fine, A.G.; Moore, D.C. Optical levitation of 10-ng spheres with nano-g acceleration sensitivity. *Phys. Rev. A.* **2017**, 96, 063841.
9. Li, W.Q.; Li, N.; Shen, Y.; Fu, Z.H.; Su, H.M.; Hu, H.Z. Dynamic analysis and rotation experiment of an optical-trapped microsphere in air. *Appl. Opt.* **2018**, 57, 823-828.
10. Taylor, M.A.; Bowen, W.P. A computational tool to characterize particle tracking measurements in optical tweezers. *J. Opt.* **2013**, 15, 085701.
11. Li, T.C.; Kheifets, S.; Raizen, M. G. Millikelvin cooling of an optically trapped microsphere in vacuum. *Nature Physics* **2011**, 7(7), 527-530.
12. Ranjit, G.; Atherton, D.P.; Stutz, J.H.; Cunningham, M.; Geraci, A.A. Attonewton force detection using microspheres in a dual beam optical trap in high vacuum. *Phys. Rev. A.* **2015**, 91, 051805.
13. Gibson1, G.M.; Leach, J.; Keen, S. Measuring the accuracy of particle position and force in optical tweezers using high-speed video microscopy. *Microscopy Research and Technique* **1999**, 44, 378–386.
14. Khorshad, A.A.; Nader, S.; Reihani, S.; Tavassoly, M.T. Moiré deflectometry-based position detection for optical tweezers. *Opt, Lett.* **2017**, 42(17), 3506-3509.
15. Gittes, F.; Schmidt, C.F. Interference model for back-focal-plane displacement detection in optical tweezers. Opt. Lett. **1998**, 23, 7-9.
16. Pralle, A.; Prummer, M.; Florin, E. L.; Stelzer, E.H.K.; Hörber, J.K.H. Three-dimensional high-resolution particle tracking for optical tweezers by forward scattered. Microsc. *Res. Techniq.* **1999**, 44, 378–386.
17. Rohrbach, A.; Stelzer, E.H.K. Three-dimensional position detection of optically trapped dielectric particles. J. Appl. Phys. **2002**, 91, 5474.
18. Nieminen, T.A.; Dunlop, H.R.; Heckenberg, N. R. Multipole expansion of strongly focused laser beams. *Journal of Quantitative Spectroscopy and Radiative Transfer* **2003**, 79, 1005–1017 .
19. Li, J. C.; Wu Y. M. Diffraction Calculation and Digital Holography I. Science Press of China, **2014**.
20. Healy, J.J.; Sheridan, J.T. Numerical approximation of scalar diffraction through first order optical systems. Proc. SPIE 7717, *Optical Modelling and Design* **2010**, 77171A.